Fabrication of Gold Nanoparticles Embedded Laser-Induced Graphene (LIG) Electrode for Hydrogen Evolution Reaction

Deepak, D., Vuruputuri, V., Bhattacharya, G., McLaughlin, J. A., & Roy, S. S. (2023). Fabrication of Gold Nanoparticles Embedded Laser-Induced Graphene (LIG) Electrode for Hydrogen Evolution Reaction. *C- Journal of Carbon Research*, *9*(4), 1-14. Article 118. Advance online publication. https://doi.org/10.3390/c9040118

Published in:
C- Journal of Carbon Research

Publication Status:
Published online: 07/12/2023

DOI:
10.3390/c9040118

Document Version
Publisher's PDF, also known as Version of record

C Journal of Carbon Research

MDPI

Article

Fabrication of Gold Nanoparticles Embedded Laser-Induced Graphene (LIG) Electrode for Hydrogen Evolution Reaction

Deepak Deepak [1,†], Vennela Vuruputuri [1,†], Gourav Bhattacharya [2,*], James A. McLaughlin [2] and Susanta Sinha Roy [1,*]

[1] Department of Physics, School of Natural Sciences, Shiv Nadar Institution of Eminence (SNIOE), Delhi-NCR, Greater Noida 201314, India; dd119@snu.edu.in (D.D.); vv652@snu.edu.in (V.V.)

[2] Nanotechnology and Integrated Bioengineering Centre, School of Engineering, Ulster University, Belfast BT15 1AP, UK; jad.mclaughlin@ulster.ac.uk

* Correspondence: g.bhattacharyasusanta.roy@snu.edu.in or g.bhattacharya@ulster.ac.uk (G.B.); susanta.roy@snu.edu.in (S.S.R.)

† These authors contribute equally to this work.

Abstract: The advancement of renewable energy technologies like water electrolysis and hydrogen fuel cells relies on the fabrication of effective and reliable catalysts for the hydrogen evolution process (HER). In this regard, we report gold nanoparticles embedded in laser-induced graphene electrodes for regulation of overpotential and electrocatalytic performance of hydrogen evolution reaction. Gold nanoparticles were deposited onto the LIG surface using electrode deposition via cyclic voltammetry (CV) at different cycle lengths. The catalyst fabrication technique enables the manipulation of many electrochemical parameters, such as overpotential value, charge transfer resistance, electrochemical active surface area, and tafel slope, through the adjustment of cyclic voltammetry (CV) cycles. The LIG-Au@50 sample demonstrates remarkable electrocatalytic characteristics, as evidenced by its low overpotential of 141 mV at a current density of 10 mA/cm^2 and reduced tafel slope of 131 mV/decade in an acidic environment. Furthermore, the presence of an augmented electrochemical active surface area, a mass activity of 8.80 A/g, and a high turnover frequency of 0.0091 s^{-1} suggest elevated and significant accessibility to plentiful active sites. A significant decrease in charge transfer resistance resulted in an enhanced rate of the water-splitting reaction.

Keywords: laser-induced graphene; gold nanoparticles; cyclic voltammetry; hydrogen evolution reaction

check for updates

Citation: Deepak, D.; Vuruputuri, V.; Bhattacharya, G.; McLaughlin, J.A.; Roy, S.S. Fabrication of Gold Nanoparticles Embedded Laser-Induced Graphene (LIG) Electrode for Hydrogen Evolution Reaction. *C* **2023**, *9*, 118. https://doi.org/10.3390/c9040118

Academic Editors: Stefano Bellucci, Nikolaos Kostoglou and Claus Rebholz

Received: 16 October 2023
Revised: 23 November 2023
Accepted: 5 December 2023
Published: 7 December 2023

1. Introduction

The rising overuse of conventional fossil fuels in recent years has severely impacted the environment, which has made using clean energy sources an urgent aspect of future sustainable development [1–3]. Hydrogen, due to its potential utilization in electrochemical processes, superior gravimetric energy density compared to conventional fuels, and its capacity to generate substantial amounts of energy, avails itself as a prominent contender among the green energy sources with the most potential in the twenty-first century [4–6]. Electrochemical splitting of water into hydrogen and oxygen, (Hydrogen/Oxygen evolution reaction) has been shown to be a renewable, effective, and ecologically benign alternative to commercial H_2 generating technologies [7]. In the context of water electrolysis, the evolution of hydrogen and oxygen occurs continuously at the anode and cathode, respectively.

$$\mathrm{HER}: 4H^+(aq) + 4e^- \rightarrow 2H_2(g) E^o = 0.0\ \mathrm{V(Reduction)} \quad (1)$$

$$\mathrm{OER}: 2H_2O(l) \rightarrow O_2 + 4H^+(aq) + 4e^- E^o = 1.23\ \mathrm{V(Oxidation)} \quad (2)$$

$$\text{Overall}: 2H_2O(l) \rightarrow O_2(g) + 2H_2(g) E^{o}_{overall} = 1.23\ V \quad (3)$$

To initiate this reaction, a voltage of 1.23 V is theoretically needed between the cathode and anode, which is 0 V (ideal) for the HER process [8,9]. For an electrochemical process to be thermodynamically favorable, an additional potential known as overpotential (η) must be supplied. The need to reduce overpotential and enhance conversion efficiency has triggered a demand for the investigation of electrocatalysts that are both abundant in the Earth's crust and possess robust hydrogen evolution reaction (HER) capabilities [10,11]. One additional obstacle involves achieving current densities of standard magnitude (10 mA/cm^2) or greater while operating at much reduced voltages, in order to scale up to industrial levels [12,13]. Therefore, the optimization of overpotential, while enhancing the reaction kinetics, holds significant implications for the overall efficiency of water splitting. Transition metals are excellent catalysts for the hydrogen evolution reaction due to their electronic structure, tunable reactivity, enriched catalytic sites and increased adsorption energies [14–16]. Typical transition metals have partially filled d orbitals, which allow them to readily interact with the electrons involved in the HER [17]. In addition, they can adsorb hydrogen atoms with moderate to high binding energies, making them efficient at both adsorbing and releasing hydrogen [18]. To date, Platinum (Pt) and Pt group catalysts have demonstrated the best catalytic activity for the HER, but their widespread use is constrained by their high cost [19,20]. Therefore, the development of effective HER electrocatalysts made of non-Pt electrode materials is still a critical issue. Gold nanoparticles have emerged as very adaptable and effective catalysts in this particular setting, presenting promising opportunities for the advancement of electrocatalysis and the production of renewable energy [21]. Quio et al. [22] reported the tunable charge transfer channels inside InSe nanosheets via suitable loading of gold nanoparticles for hydrogen evolution reactions. In a similar report, Tran et al. [23] depicted excellent HER activity for gold nanoparticles with a low overpotential value of 200 mV at a higher turnover frequency. In another work, Zhao et al. [24] examined the impact of elevated doping concentrations of gold in the Au-MoS_2 composite. The composite material showed a notable enhancement in catalytic activity when compared to the pure MoS_2. Nevertheless, it is worth noting that single-phase transition metals have suboptimal catalytic activity and a deficiency in stability, resulting in limited catalytic activity. Thus, the synthesis of a network of hybrid electrocatalysts, as opposed to relying solely on conventional single-phase approaches can open several doors to fabricate high current density catalysts with low overpotential values. This can be achieved by sufficient doping of heteroatoms, surface modification and phase engineering regulation [25]. Carbon materials, including carbon nanotubes (CNTs) and graphene, are frequently employed as support for metal catalysts, such as platinum (Pt), nickel (Ni), gold (Au) and cobalt (Co), in the context of the hydrogen evolution reaction (HER) [26,27]. One such substrate is LIG film, which is an amorphous form of carbon and can be synthesized by directing a CO_2 laser on carbon materials [28]. Metal nanoparticles on the LIG catalyst surface experience improved dispersion and stability due to the presence of increased surface area and favorable electrical conductivity [29]. Besides the porous structure, LIG exhibits exceptional electrical conductivity, thereby promoting efficient electron transport during the process of the hydrogen evolution reaction (HER) [30,31]. Therefore, fabricating catalyst which is a hybrid of gold nanoparticles and LIG can access enlarged current densities to minimize the overpotential values. With this in mind, this work aims to examine the catalytic efficiency of heterostructures composed of LIG and gold nanoparticles for hydrogen evolution reaction (HER) in an acidic environment. The process of depositing gold nanoparticles onto the surface of LIG was achieved through electrode deposition employing cyclic voltammetry (CV) with varying cycle durations (20, 50 and 100 cycles). The catalytic efficiency of the electrodes was observed to first increase with the concentration of gold nanoparticles, with maximum at moderate level. Among the samples, the one prepared using 50 CV cycles (LIG-Au@50) demonstrated the lowest overpotential (145 mV at 10 mA/cm^2) with a minimum tafel slope value of 131 mV/decade.

As-fabricated LIG-Au@50 exhibit the highest double layer capacitance value leading to the highest electrochemical active surface area along with best turnover frequency value of 0.0043 s^{-1}. The distinctive performance exhibited by the LIG-gold heterostructure renders it a highly promising nominee for hydrogen production through electrolysis.

2. Experimental Section

2.1. Materials and Methods

Tetra chloroauric acid ($HAuCl_4 \cdot 4H_2O$), sulphuric acid (H_2SO_4), carbon black, Polyvinylidene fluoride (PVDF), N-Methyl-2-pyrrolidone (NMP), were purchased from Sigma Aldrich. Kapton film (Film, 5 Mil, no adhesive, 12″*12″) was purchased from Cole Parmer The chemicals were used as purchased. Nickel foam (NF) was purchased from Global Nanotech and used as a substrate. The fabrication of LIG was aided by the MV laser CW 6040 laser engraving machine.

Fabrication of Laser-Induced Graphene Film-Based Gold Nanocomposites

The fabrication of LIG on the Kapton (polyimide (PI)) sheet was achieved by using a CO_2 laser cutting and engraving equipment operating at a wavelength of 10.6 µm. Prior to the fabrication process, the PI sheets underwent a comprehensive rinsing procedure with ethanol and water. As synthesized LIG was used as the working electrode in a 3-electrode cell, comprising of an Ag/AgCl reference electrode, and a platinum counter electrode. The electrolyte solution was prepared by dissolving 5 mM $HAuCl_4$ in 1 mM H_2SO_4. The gold nanoparticles were deposited onto the LIG surface using cyclic voltammetry (CV) for 20, 50, and 100 cycles, in a voltage window of −0.3 V to 0.6 V (Figure S4). The working electrode was then dried and scratched to obtain the Au-LIG nanocomposites. A total of 5 mg of synthesized nanostructures were mixed with 5% carbon black with a dropwise addition of NMP and 5% PVDF to obtain a slurry which was further coated on nickel foam with an active area of 1 cm^2. This slurry was pasted onto a nickel foam and dried to obtain the electrocatalysts. The schematic of the whole process is shown in Figure 1. The geometrical area for each electrode was kept as 1 cm × 1 cm.

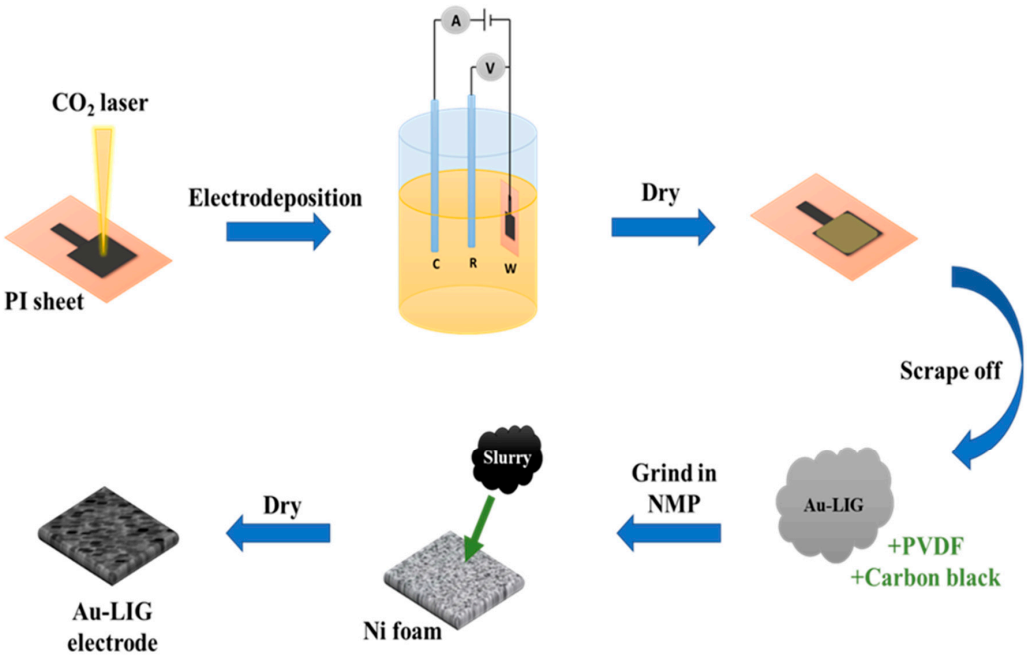

Figure 1. Schematic representation of the synthesis of LIG followed by fabrication of LIG-Au nanostructures on nickel foam.

2.2. Characterization Details

XRD of as-synthesized samples was investigated in coupled θ-2θ diffraction (Bruker D8 discover, Karlsruhe, Germany) using Cu-Kα radiation. Surface morphology was studied using FESEM JEOL JSM 7600 PLUS ,Tokyo, Japan). The water contact angle was measured using a contact-angle-measuring system (APEX, Delhi, India).

2.3. Electrochemical Measurement Details

All electrochemical results were analyzed using an Autolab potentiostat/galvanostat 302N instrument (Metrohm B.V. Utrecht, The Netherlands) controlled by Nova (version 1.10) software. The catalysis activity of the nanostructures was investigated in three-electrode set-ups with Ag/AgCl as the reference electrode, platinum (Pt) as the counter electrode and hybrid nanostructures catalyst as the working electrode. All measurements were taken in acidic media of 0.5 M H_2SO_4 solution. Linear sweep voltammetry (LSV) tests were conducted in the range of 0 to −0.4 V at a scan rate of 5 mV/s. EIS results were performed in a frequency range of 0.01 Hz to 10KHz. Potential vs. Ag/AgCl were converted using the formula E(RHE) = E(Ag/AgCl) + 0.059 × pH + 0.197. Here RHE represents a reversible hydrogen electrode. All overpotentials reported in the current study are concerning the RHE. Cyclic Voltammetry tests were performed from −0.1 V to 0.05 V to calculate the double-layer capacitance.

3. Results

3.1. XRD Analysis

X-ray diffraction technique is used to examine the crystal phase and plane orientation of as-synthesized LIG and nanostructure films. Figure S1 represents the XRD pattern of pristine LIG, which shows the characteristic peaks at a 2θ value of 26.5°. The observed peak can be attributed to the (002) crystallographic planes of graphitic carbon [32]. Figure 2a shows the XRD spectra of LIG-Au nanocomposites, which confirms the presence of gold nanoparticles inside the graphene matrix. The dominant peaks of gold nanoparticles are indicative of the face-cantered cubic (FCC) crystal structure of gold. In the case of FCC gold, prominent peaks may be observed at 38.2°, 44.4°, 64.6°, and 77.6°, as indicated by the 2θ values. The aforementioned crystallographic planes are denoted as (111), (200), (220), and (311), respectively [33,34]. No peak other than gold and graphene was depicted, which further confirms the successful synthesis of LIG-Au nanocomposites.

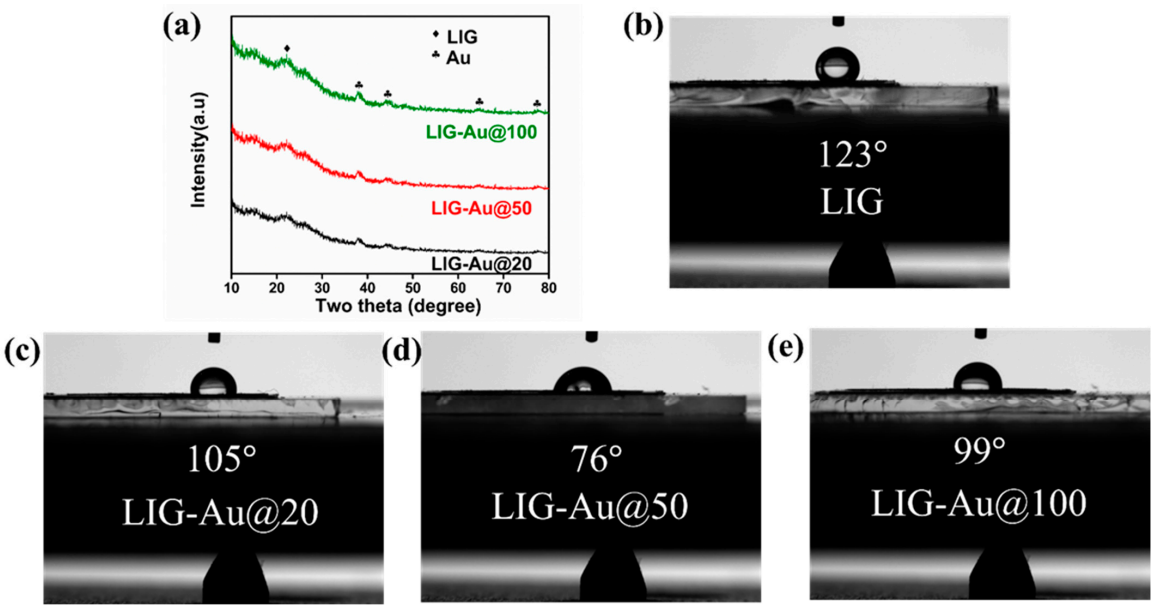

Figure 2. (**a**) shows the XRD pattern of fabricated LIG-Au nanostructures (**b**–**e**) water contact angle variation of LIG, LIG-Au@20, LIG-Au@50 and LIG-Au@100, respectively.

3.2. Contact Angle Measurements

The assessment of wettability between a liquid and a solid surface is commonly conducted by contact angle measurements, which serve as a beneficial approach in this regard. This measurement offers valuable insights into the interplay between a liquid and a solid, a factor of utmost importance in electrochemistry which explains and support certain cause [35]. Figure 2b–e represents contact angle measurements of pristine LIG, LIG-Au@20, 50, and 100, respectively. Pristine LIG is prone to hydrophobic behavior (123°) due to the presence of a non-polar carbon-carbon (C-C) bond chain. However, gold being a metal, is more liable towards hydrophilicity, which can be a real asset in regulating the electrocatalytic properties. It is evident that LIG-Au@20 and 100 exhibit lower contact angles of 105° and 99°, respectively, as compared to LIG due to a certain amount of Au loading. LIG-Au@50, which has a moderate level of gold concentration, shows the lowest contact angle of 76°, being responsible for excellent electrochemical performances. As the loading amount of gold increases after 50 cycles, there is a possible agglomeration of gold nanoparticles covering the LIG surface which can be observed from FESEM. Radiom et al. [36] demonstrated that the contact angle increases when nanoparticles agglomerate or when their concentration exceeds a particular threshold over time. This phenomenon can be explained through two mechanisms: a decrease in the wetting transition as a result of a reduced particle count on the outermost edge of the film due to agglomeration, or the strong adsorption of nanoparticles onto the film's surface. Due to the significant agglomerations observed in LIG-Au@100, the contact angle will probably be greater when compared to LIG-Au@50. In another aspect, Mamdouh et al. [37] controlled the wetting behaviour of electrodeposited gold films. As the surface coverage increases, there is a possible enhancement in gold thickness and the wetting transition from hydrophilic to hydrophobic takes place after certain threshold values.

3.3. SEM Analysis

Scanning electron microscopy (SEM) can be employed to investigate the morphology of LIG and LIG-Au nanocomposites, facilitating the comprehension of their microstructural characteristics and surface attributes. Figure S2a represents the FESEM image of pristine LIG film, revealing a multitude of minute pores and voids dispersed over the material. The presence of these pores significantly contributes to the electrochemical active surface area of LIG, rendering it well-suited for electrocatalytic performance. Figure 3a–c shows the surface morphology of LIG-Au@20, 50 and 100 samples. The LIG-Au nanocomposites demonstrate a significant distribution of gold nanoparticles across the porous LIG surface, even when the size and loading quantity of the gold nanoparticles increase during cyclic voltammetry (CV) cycles. The LIG-Au@20 (Figure 3a) and LIG-Au@50 (Figure 3b) samples exhibit the presence of gold nanoparticles distributed across the surface of the LIG material, with a slight variation in the size of the nanoparticle clusters. In contrast, LIG-Au@100 (Figure 3c) displays significant agglomeration throughout the whole surface, which can result in an inferior electrocatalytic performance compared to the other two samples. The inset of Figure 3a–c shows the EDS spectrum to further confirm the composition of samples which indicates a qualitative consistency in the gold content with the CV cycles. Figure 3d shows the size distribution histogram of lig-Au@50 calculated from FESEM. Figure 3e–h represents the qualitative elemental mapping analysis to identify the phase distribution among the composite structure.

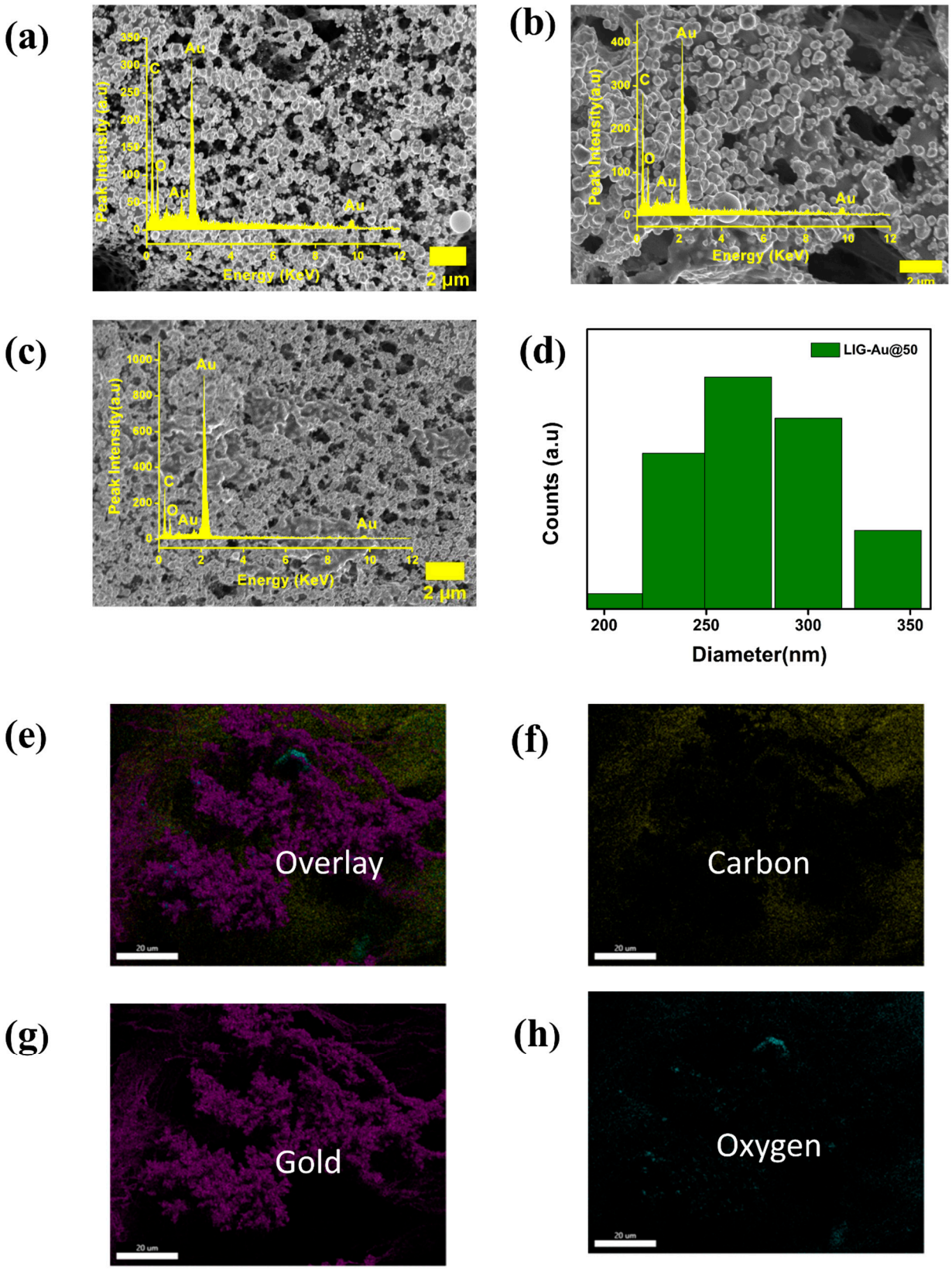

Figure 3. (**a**–**c**) Surface morphology analysis through FESEM of LIG-Au@20, LIG-Au@50, and LIG-Au@100 with inset shows qualitative EDS spectrum (**d**) size distribution histogram for LIG-Au@50 (**e**–**h**) elemental mapping of LIG-Au@50.

3.4. Electrochemical Performance

The electrocatalytic performance was assessed through the implementation of linear sweep voltammetry experiments in a conventional three-electrode setup. The reference electrode employed was Ag/AgCl, while platinum was utilized as the counter electrode. The experiments were conducted in a 0.5 M H_2SO_4 solution. The investigation of the hydrogen evolution reaction occurring at the surface of the samples can be conducted by considering several parameters, including the tafel slope, overpotential, electrochemical active surface area, mass activity, and turnover frequency.

The Tafel slope can be calculated by the following equation.

$$\eta = b.\log\left(\frac{j}{j_0}\right) \tag{4}$$

where, η, j, j_0 and b are the overpotential, current density, exchange current density and tafel slope [38,39].

Overpotential η can be obtained by following the equation:

$$\eta = E(E\ vs\ RHE) + 0.197 + 0.059 \times pH \tag{5}$$

The turnover frequency (TOF) values for the fabricated catalyst can be obtained by following the equation [38,39]

$$\text{TOF} = j \times \frac{S}{2 \times F \times n} \tag{6}$$

where j is the current density measured at the 200 mV overpotential, S is the electrode's surface area (1 cm^2), F is the Faraday efficiency (96,485 C mol^{-1}), and n is the number of moles of catalyst.

The mass activity of the hybrid catalyst can be estimated by the following equation:

$$\text{Mass Activity} = \frac{I}{m} \tag{7}$$

where m is the entire mass loading on the electrode, and I is the current equivalent to −0.4 V versus RHE [38,39].

To determine the electrochemical surface area (ECSA) the following equation can be used:

$$\text{ECSA} = \frac{S \times C_{dl}}{C_s} \tag{8}$$

where C_{dl} and C_s represent the double-layer capacitance obtained from CV scans and capacitance of the electrode, respectively, and S is the geometrical surface area of the fabricated electrode [38,39].

The fabricated electrocatalysts demonstrate remarkable electrocatalytic activity for the hydrogen evolution reaction (HER). Notably, LIG-Au@50 demonstrates superior performance as a host for active sites and excellent catalysis activity. LIG exhibits exceptional electrical conductivity, rendering it a very proficient conductor and its amalgamation with gold nanoparticles enhances the total catalytic conductivity [40]. The significance of these nanostructures lies in the indispensability of effective electron transport for the process of hydrogen evolution reaction (HER). The interplay between gold and graphene has the potential to provide synergistic outcomes that augment the catalytic efficacy of both substances [41]. HER process can proceed via either the Volmer–Heyrovsky step or the Volmer–Tafel step [42]:

$$H^+ + M^* + e^- \rightarrow H^{M^*} \qquad \text{Volmer step}$$

$$M^* + H^+ + e^- + H^{M^*} \rightarrow H_2 + M^* \qquad \text{Heyrovsky step}$$

$$2H^{M*} \rightarrow H_2 + 2M^* \qquad \text{Tafel step}$$

where M* represents the active site on the surface of LIG-Au nanostructures.

Figure 4a represents the LSV curve of pristine LIG and LIG-Au nanocomposite materials at a scan rate of 5 mV/s. The hybrid nanostructures of catalysts exhibited lower overpotential values compared to the bare LIG and LIG-Au nanocomposites. Among these hybrid structures, LIG-Au@50 demonstrated the lowest overpotential of 141 mV (vs. RHE) at a current density of 10 mA/cm^2 which is promising for potential future applications. Figure 4b presents a bar diagram that demonstrates a comparative study of overpotential values. The Tafel slope is a parameter that offers insights into the kinetics of the hydrogen evolution reaction. The steeper the tafel slope, the faster the reaction kinetics [43].

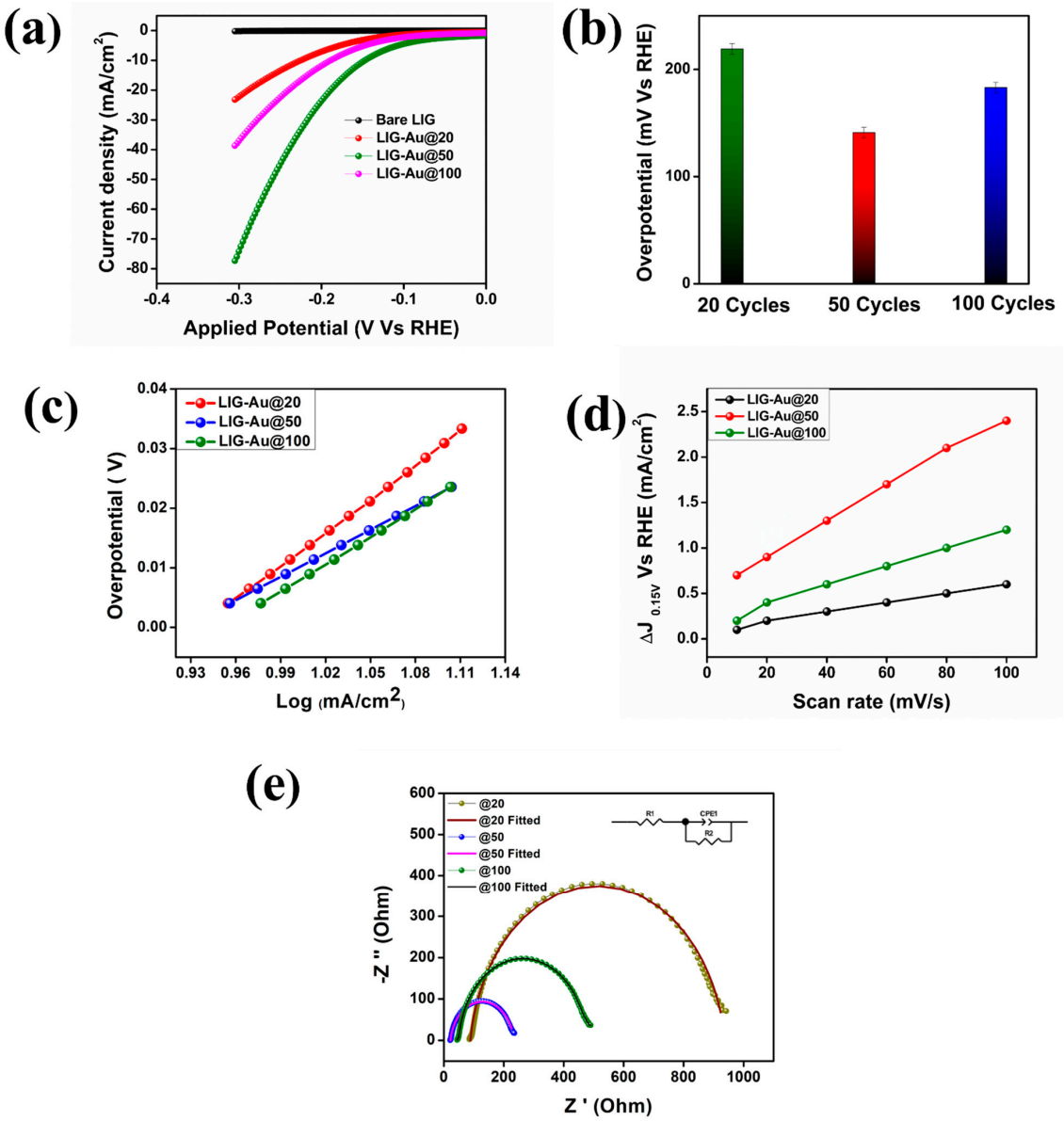

Figure 4. Electrochemical performance of hybrid catalysts. (**a**) LSV scans from 0 V to −0.4 V (vs. RHE) at a scan rate of 5 mV/s (**b**) bar diagram representing the overpotential values of different materials (**c**) different tafel plots of the catalyst evaluate the kinetic process (**d**) C_{dl} values calculated at 1.5V vs. RHE using CV scans for calculation of electrochemically active surface area (**e**) corresponding EIS spectra of all samples.

Figure 4c represents tafel slope variations for LIG-Au nanostructures. The LIG-Au@50 sample showed a tafel slope of 131 mV/decade which is lowest in comparison to LIG-Au@20 and LIG-Au@100 indicating better and faster catalysis activity. In addition, the phenomenon of double-layer capacitance offers valuable insights into the number of active sites and is employed in the determination of the electrochemically active surface area. Figure S3 shows the different cyclic voltammetry scans from −0.1 V to 0.05 V to calculate the double layer capacitance (C_{dl}) of all hybrids in 0.5 M H_2SO_4 solution. Electrochemical active surface area was calculated to understand the mechanism of catalytic activity for all materials and found in the order of LIG-Au@50 > LIG-Au@100 > LIG-Au@20 with values of 1.28 cm^2 > 0.76 cm^2 > 0.30 cm^2.

A qualitative comparison of CV scans in 0.5 M H_2SO_4 of all samples is shown in Figure 4d. The excellent value of ECSA for LIG-Au@50 (1.28 cm^2) depicts a large number of available exposed locations for catalytic activity. Turnover frequency (TOF) pertains to the assessment of the number of hydrogen molecules generated per active catalytic site within a given time interval [44]. A greater TOF value signifies a more effective catalyst, a crucial factor for the use of the catalyst in real scenarios. It is observed that the LIG-Au@50 catalyst had a TOF value of 0.009 s^{-1} which is higher than the other materials (Table S1). Furthermore, the mass activities of the catalysts were determined using Equation (7). The obtained values indicate that the LIG-Au@50 exhibits superior performance, which is consistent with the findings of prior studies. Table 1 displays the performance metrics of all HER catalysts. Electrochemical impedance spectroscopy (EIS) has the capability to offer significant insights into the kinetics of the hydrogen evolution reaction (HER), specifically pertaining to the charge transfer resistance occurring at the interface between the electrode and electrolyte [45,46]. The lower the charge transfer, the faster will be the kinetic process. Figure 4e shows EIS spectra of fabricated catalysts in a frequency range of 0.01 Hz to 10 KHz. The inset of the graph represents the equivalent fitted circuit evaluating the values of charge transfer and solution resistance values. R_2 represents the charge transfer resistance offered at the electrode electrolyte interface whereas R_1 shows the solution resistance value. LIG-Au@50 offered the least Rct value as compared to 20 and 100 cycles. In the case of LIG-Au@50, the gold nanoparticles uniformly cover the LIG surface with no possibility of agglomeration leading to easy access to ionic movement. However, LIG-Au@100 consists of larger gold chunks which are further agglomerated causing difficulty for the movements of ions throughout. This phenomenon leads to the increase in the charge transfer resistance of LIG-Au@100 in comparison to 20 and 50 cycles and is also responsible for poorer catalytic activity.

Table 1. Electrochemical performance parameters of LIG-Au nanocomposites.

S.No.	Sample Name	Overpotential (η_{10}) (mV)	Tafel Slope (mVdec^{-1})	ECSA (cm^2)	Mass Activity (A g^{-1})	TOF (s^{-1})
1	LIG-Au@20	219	187	0.30	2.09	0.00027
2	LIG-Au@50	141	131	1.28	8.80	0.0091
3	LIG-Au@100	183	154	0.76	4.29	0.0045

The least R_{ct} and R_s values of LIG-Au@50 support better catalytic activity over other samples. Table 2 represents a qualitative comparison of EIS performance parameters for all three nanostructures. To check the practical applicability of the fabricated catalysts, LSV measurements were further carried out with a symmetric configuration setup (Figure 5a) in which the LIG-Au@50 acts as both anode and cathode. The symmetric device setup displayed an overpotential value of 382 mV at 10 mA/cm^2. A stability test was conducted to check the robustness of the as-fabricated LIG-Au@50 electrode through 1000 CV scans and recording the overpotential values before and after measurements (Figure 5b). The difference in the overpotential values was found to be 13 mV which is notably much less indicating the decent stability of the electrode. Figure 5c shows the chronopotentiometry

test at 50 mA/cm^2 for 50 h to check the overpotential fluctuations. Table 3 Comparison of performance parameters of LIG-Au@50 catalyst with similar materials previously reported in the literature.

Table 2. EIS performance parameters of as-fabricated catalysts.

Sample	Charge Transfer Resistance (ohm)	Solution Resistance (ohm)
LIG-Au@20	848.5	88.67
LIG-Au@50	211.9	22.19
LIG-Au@100	440.8	46.16

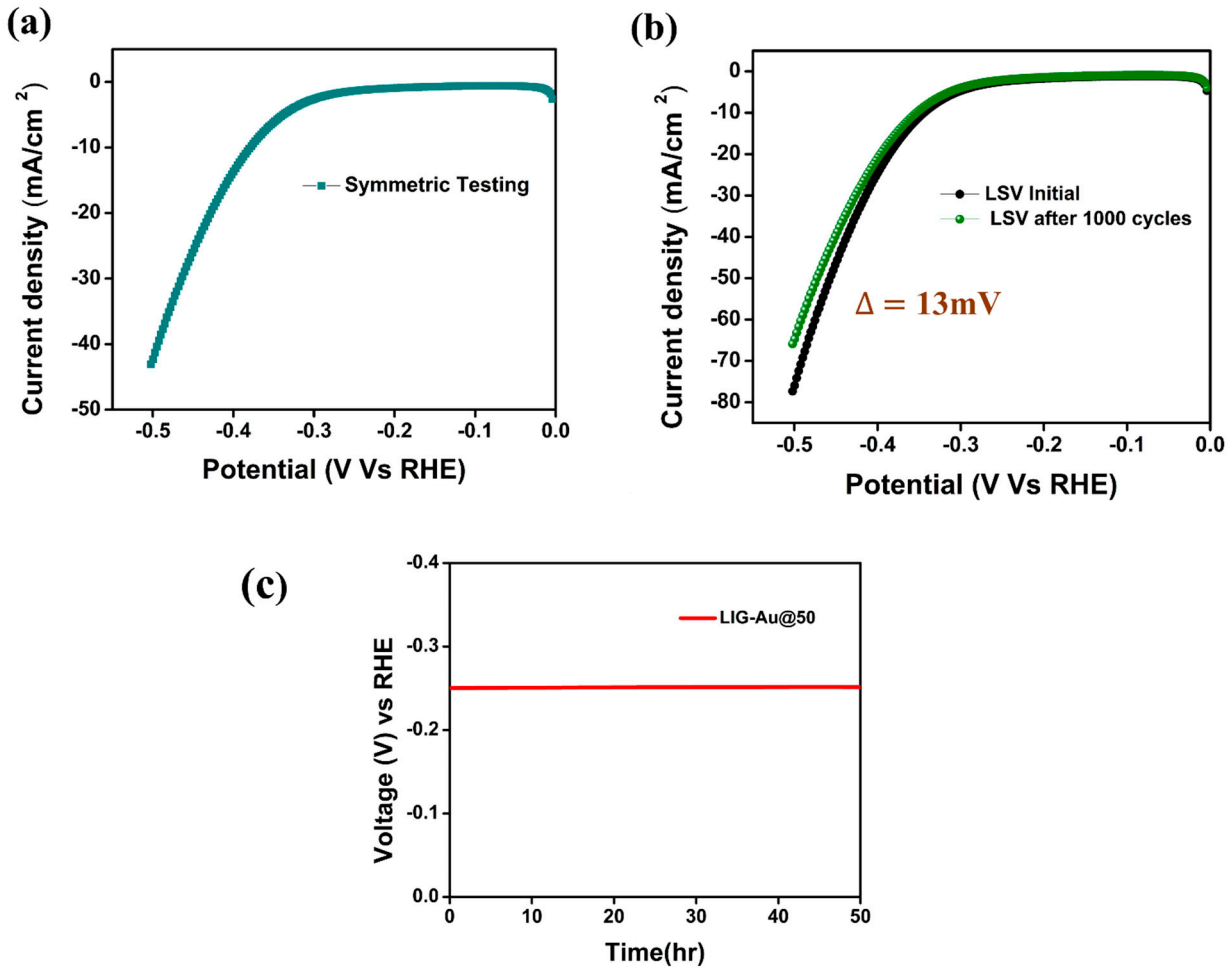

Figure 5. (**a**) LSV scan of a symmetric device fabricated using LIG-Au@50 electrode (**b**) CV scan was used to check the stability of the LIG-Au@50 catalysis over 1000 cycles of continuous operation (**c**) chronopotentiometry test at 50 mA/cm^2 for 50 h.

Table 3. Comparison of performance parameters of LIG-Au@50 catalyst with similar materials previously reported in the literature.

S.No.	Catalyst	Electrolyte	Overpotential at 10 mA/cm^2 (mV)	Reference
1	Gold nanoparticles	0 pH H_2SO_4	200	[23]
2	InSe Au	0.5 M H_2SO_4	392	[22]
3	LIG-CuO	1M KOH	149	[47]
4	LIG-Mos_2	0.5 M H_2SO_4	216	[48]
5	Pt 3D LIG	1 M KOH	455	[49]
6	**LIG-Au@50**	**0.5 M H_2SO_4**	**141**	**Present work**

4. Discussion

In addition to the aforementioned findings, the exceptional electrocatalytic performance of LIG-Au@50 can be substantiated based on the following features:

(1) The utilization of nickel foam as a substrate results in the establishment of robust interfacial contact with the active materials. The objective is to decrease the interfacial resistance and enhance the kinetics of charge transfer [50].

(2) The measurement of the contact angle can yield valuable insights into the availability and accessibility of the active sites present on the surface of the electrode. A surface exhibiting a reduced contact angle is inclined to possess a larger proportion of its surface area that is accessible to the electrolyte [51]. An enlarged electrochemically active surface area (ECSA) often leads to enhanced catalytic activity in the hydrogen evolution reaction (HER). The least water contact angle of LIG-Au@50 among others supports its better catalytic activity.

(3) The interplay between gold nanoparticles and laser-induced graphene has the potential to provide synergistic outcomes that augment the catalytic efficacy of both substances at moderate level of gold concentration (50 cycles). An increased quantity of gold on the (LIG) surface, specifically after 100 cycles, induces significant agglomeration, hence diminishing the catalytic activity. Conversely, a lower quantity of gold on the LIG surface, particularly after 20 cycles, exhibits an inadequate number of active sites for catalytic reactions.

5. Conclusions

In summary, this study reported the fabrication of gold nanoparticles embedded in a laser-induced graphene electrode for hydrogen evolution reaction using the electrodeposition method resulting in uniform coverage of gold over the LIG surface at a moderate CV cycling rate which further facilitates mass transport and charge transfer properties. The fabricated catalysts exhibited remarkable electrocatalytic performance, characterized by a low overpotential value of 141 mV at a current density of 10 mA/cm^2, as well as a significantly high electrochemical active surface area of 1.28 cm^2 suggesting the catalysts hold great potential in comparison to other materials of similar nature. The interaction between gold nanoparticles and laser-induced graphene possesses the capacity to yield synergistic effects that enhance catalytic efficiency. Such electrode material offers new insights into the advancement of catalysts that are highly active, stable, and cost-effective, thereby addressing the requirements of commercial electrolysis technology.

Supplementary Materials: The following supporting information can be downloaded at: https://www.mdpi.com/article/10.3390/c9040118/s1, XRD, Raman and SEM of LIG, CV curves at different scan rates, CV cycles of electrodeposition, (LSV at 2 mV/s (Figures S1–S6)). Figure S1 shows the XRD pattern of bare LIG. Figure S2 (a) represents FESEM of bare LIG (b) Raman spectra depicting D, G and 2D peaks of LIG. Figure S3 (a) shows the CV scan in the non-faradic region to calculate the double layer capacitance in 0.5M H_2SO_4 solution. (b–d) represents the individual CV scans in the same regions for all LIG-Au nanostructures. Figure S4 represents the CV scans of bare LIG in HauCl4 and H_2SO_4 solution during the electrodeposition process at different cycles. Figure S5 Cyclic Voltammetry studies of LIG-Au nanostructures in the presence of 5mM Ferro/Ferricyanide + 0.1M KCl. Figure S6 LSV scans at 2 mV/s. Table S1 shows the TOF values for comparison of LIG-Au@50 with other similar catalysis [52,53].

Author Contributions: All authors have contributed sufficiently to the work. D.D.: Conceptualization, Methodology, Validation, Writing—original draft, Writing—review &editing; V.V.: Conceptualization, Methodology, Validation, Writing—original draft, Writing—review & editing; G.B.: Methodology, Validation, data curation, Investigation, Writing—review & editing; J.A.M.: Conceptualization, Methodology, Validation, Investigation, Data curation; S.S.R.: Conceptualization, Methodology, Validation, Investigation, Data curation, Writing—review & editing, Supervision. All authors have read and agreed to the published version of the manuscript.

Funding: This research received no external funding.

Data Availability Statement: Data are contained within the article.

Acknowledgments: Deepak Deepak acknowledges Shiv Nadar Institution of Eminence (SNIoE), India for the financial support through scholarship.

Conflicts of Interest: The authors declare that they have no conflict of interest.

References

1. Liu, L.; Cheng, S.Y.; Li, J.B.; Huang, Y.F. Mitigating Environmental Pollution and Impacts from Fossil Fuels: The Role of Alternative Fuels. *Energy Sources Part A Recovery Util. Environ. Eff.* **2007**, *29*, 1069–1080. [CrossRef]
2. Jaiswal, K.K.; Chowdhury, C.R.; Yadav, D.; Verma, R.; Dutta, S.; Jaiswal, K.S.; Sangmesh, B.; Karuppasamy, K.S.K. Renewable and Sustainable Clean Energy Development and Impact on Social, Economic, and Environmental Health. *Energy Nexus* **2022**, *7*, 100118. [CrossRef]
3. Abbasi, T.; Abbasi, S.A. Biomass Energy and the Environmental Impacts Associated with Its Production and Utilization. *Renew. Sustain. Energy Rev.* **2010**, *14*, 919–937. [CrossRef]
4. Staffell, I.; Scamman, D.; Velazquez Abad, A.; Balcombe, P.; Dodds, P.E.; Ekins, P.; Shah, N.; Ward, K.R. The Role of Hydrogen and Fuel Cells in the Global Energy System. *Energy Environ. Sci.* **2019**, *12*, 463–491. [CrossRef]
5. Wei, C.; Rao, R.R.; Peng, J.; Huang, B.; Stephens, I.E.L.; Risch, M.; Xu, Z.J.; Shao-Horn, Y. Recommended Practices and Benchmark Activity for Hydrogen and Oxygen Electrocatalysis in Water Splitting and Fuel Cells. *Adv. Mater.* **2019**, *31*, 1806296. [CrossRef] [PubMed]
6. Peng, X.; Pi, C.; Zhang, X.; Li, S.; Huo, K.; Chu, P.K. Recent Progress of Transition Metal Nitrides for Efficient Electrocatalytic Water Splitting. *Sustain. Energy Fuels* **2019**, *3*, 366–381. [CrossRef]
7. Sahin, N.E.; Pech-Rodríguez, W.J.; Meléndez-González, P.C.; Lopez Hernández, J.; Rocha-Rangel, E. Water Splitting as an Alternative for Electrochemical Hydrogen and Oxygen Generation: Current Status, Trends, and Challenges. *Energies* **2023**, *16*, 5078. [CrossRef]
8. Li, Y.; Chen, J.; Cai, P.; Wen, Z. An Electrochemically Neutralized Energy-Assisted Low-Cost Acid-Alkaline Electrolyzer for Energy-Saving Electrolysis Hydrogen Generation. *J. Mater. Chem. A* **2018**, *6*, 4948–4954. [CrossRef]
9. Yu, X.; Araujo, R.B.; Qiu, Z.; Campos dos Santos, E.; Anil, A.; Cornell, A.; Pettersson, L.G.M.; Johnsson, M. Hydrogen Evolution Linked to Selective Oxidation of Glycerol over $CoMoO_4$—A Theoretically Predicted Catalyst. *Adv. Energy Mater.* **2022**, *12*, 2103750. [CrossRef]
10. Sarkar, S.; Peter, S.C. An Overview on Pd-Based Electrocatalysts for the Hydrogen Evolution Reaction. *Inorg. Chem. Front.* **2018**, *5*, 2060–2080. [CrossRef]
11. Wu, H.; Feng, C.; Zhang, L.; Zhang, J.; Wilkinson, D.P. Non-Noble Metal Electrocatalysts for the Hydrogen Evolution Reaction in Water Electrolysis. *Electrochem. Energy Rev.* **2021**, *4*, 473–507. [CrossRef]
12. Ibn Shamsah, S.M. Earth-Abundant Electrocatalysts for Water Splitting: Current and Future Directions. *Catalysts* **2021**, *11*, 429. [CrossRef]
13. Zhou, Q.; Liao, L.; Zhou, H.; Li, D.; Tang, D.; Yu, F. Innovative Strategies in Design of Transition Metal-Based Catalysts for Large-Current-Density Alkaline Water/Seawater Electrolysis. *Mater. Today Phys.* **2022**, *26*, 100727. [CrossRef]
14. Zhang, J.; Liu, Y.; Sun, C.; Xi, P.; Peng, S.; Gao, D.; Xue, D. Accelerated Hydrogen Evolution Reaction in CoS_2 by Transition-Metal Doping. *ACS Energy Lett.* **2018**, *3*, 779–786. [CrossRef]
15. Zhang, L.; Liu, W.; Dou, Y.; Du, Z.; Shao, M. The Role of Transition Metal and Nitrogen in Metal–N–C Composites for Hydrogen Evolution Reaction at Universal PHs. *J. Phys. Chem. C* **2016**, *120*, 29047–29053. [CrossRef]
16. Jin, H.; Liu, X.; Chen, S.; Vasileff, A.; Li, L.; Jiao, Y.; Song, L.; Zheng, Y.; Qiao, S.-Z. Heteroatom-Doped Transition Metal Electrocatalysts for Hydrogen Evolution Reaction. *ACS Energy Lett.* **2019**, *4*, 805–810. [CrossRef]
17. Mott, N.F. The Basis of the Electron Theory of Metals, with Special Reference to the Transition Metals. *Proc. Phys. Soc. Sect. A* **1949**, *62*, 416. [CrossRef]
18. Song, J.; Zhu, C.; Xu, B.Z.; Fu, S.; Engelhard, M.H.; Ye, R.; Du, D.; Beckman, S.P.; Lin, Y. Bimetallic Cobalt-Based Phosphide Zeolitic Imidazolate Framework: CoP_x Phase-Dependent Electrical Conductivity and Hydrogen Atom Adsorption Energy for Efficient Overall Water Splitting. *Adv. Energy Mater.* **2017**, *7*, 1601555. [CrossRef]
19. Shi, Y.; Ma, Z.-R.; Xiao, Y.-Y.; Yin, Y.-C.; Huang, W.-M.; Huang, Z.-C.; Zheng, Y.-Z.; Mu, F.-Y.; Huang, R.; Shi, G.-Y.; et al. Electronic Metal–Support Interaction Modulates Single-Atom Platinum Catalysis for Hydrogen Evolution Reaction. *Nat. Commun.* **2021**, *12*, 3021. [CrossRef]
20. Selvaraj, V.; Alagar, M. Pt and Pt–Ru Nanoparticles Decorated Polypyrrole/Multiwalled Carbon Nanotubes and Their Catalytic Activity towards Methanol Oxidation. *Electrochem. Commun.* **2007**, *9*, 1145–1153. [CrossRef]
21. Wang, Y.; Sun, Y.; Liao, H.; Sun, S.; Li, S.; Ager, J.W.; Xu, Z.J. Activation Effect of Electrochemical Cycling on Gold Nanoparticles towards the Hydrogen Evolution Reaction in Sulfuric Acid. *Electrochim. Acta* **2016**, *209*, 440–447. [CrossRef]
22. Qiao, H.; Li, Z.; Liu, F.; Ma, Q.; Ren, X.; Huang, Z.; Liu, H.; Deng, J.; Zhang, Y.; Liu, Y.; et al. Au Nanoparticle Modification Induces Charge-Transfer Channels to Enhance the Electrocatalytic Hydrogen Evolution Reaction of InSe Nanosheets. *ACS Appl. Mater. Interfaces* **2022**, *14*, 2908–2917. [CrossRef] [PubMed]

23. Tran, T.D.; Nguyen, M.T.T.; Le, H.V.; Nguyen, D.N.; Truong, Q.D.; Tran, P.D. Gold Nanoparticles as an Outstanding Catalyst for the Hydrogen Evolution Reaction. *Chem. Commun.* **2018**, *54*, 3363–3366. [CrossRef] [PubMed]
24. Zhao, X.; He, D.-W.; Wang, Y.-S.; Fu, C. In Situ Growth of Different Numbers of Gold Nanoparticles on MoS_2 with Enhanced Electrocatalytic Activity for Hydrogen Evolution Reaction. *Chin. Phys. B* **2018**, *27*, 68103. [CrossRef]
25. Shi, Y.; Zhou, Y.; Yang, D.-R.; Xu, W.-X.; Wang, C.; Wang, F.-B.; Xu, J.-J.; Xia, X.-H.; Chen, H.-Y. Energy Level Engineering of MoS_2 by Transition-Metal Doping for Accelerating Hydrogen Evolution Reaction. *J. Am. Chem. Soc.* **2017**, *139*, 15479–15485. [CrossRef] [PubMed]
26. Zhang, H.-X.; Li, Y.; Li, M.-Y.; Zhang, H.; Zhang, J. Boosting Electrocatalytic Hydrogen Evolution by Plasmon-Driven Hot-Electron Excitation. *Nanoscale* **2018**, *10*, 2236–2241. [CrossRef] [PubMed]
27. Zhang, W.; Xi, R.; Li, Y.; Zhang, Y.; Wang, P.; Hu, D. Recent Development of Transition Metal Doped Carbon Materials Derived from Biomass for Hydrogen Evolution Reaction. *Int. J. Hydrogen Energy* **2022**, *47*, 32436–32454. [CrossRef]
28. Ye, R.; James, D.K.; Tour, J.M. Laser-Induced Graphene. *Acc. Chem. Res.* **2018**, *51*, 1609–1620. [CrossRef]
29. Hui, X.; Xuan, X.; Kim, J.; Park, J.Y. A Highly Flexible and Selective Dopamine Sensor Based on Pt-Au Nanoparticle-Modified Laser-Induced Graphene. *Electrochim. Acta* **2019**, *328*, 135066. [CrossRef]
30. Zhang, J.; Zhang, C.; Sha, J.; Fei, H.; Li, Y.; Tour, J.M. Efficient Water-Splitting Electrodes Based on Laser-Induced Graphene. *ACS Appl. Mater. Interfaces* **2017**, *9*, 26840–26847. [CrossRef]
31. Kucherenko, I.S.; Chen, B.; Johnson, Z.; Wilkins, A.; Sanborn, D.; Figueroa-Felix, N.; Mendivelso-Perez, D.; Smith, E.A.; Gomes, C.; Claussen, J.C. Laser-Induced Graphene Electrodes for Electrochemical Ion Sensing, Pesticide Monitoring, and Water Splitting. *Anal. Bioanal. Chem.* **2021**, *413*, 6201–6212. [CrossRef] [PubMed]
32. Ye, R.; James, D.K.; Tour, J.M. Laser-Induced Graphene: From Discovery to Translation. *Adv. Mater.* **2019**, *31*, 1803621. [CrossRef] [PubMed]
33. Sneha, K.; Esterle, A.; Sharma, N.; Sahi, S. Yucca-Derived Synthesis of Gold Nanomaterial and Their Catalytic Potential. *Nanoscale Res. Lett.* **2014**, *9*, 627. [CrossRef]
34. Khalil, M.; Ismail, E.; El-Magdoub, F. Biosynthesis of Au Nanoparticles Using Olive Leaf Extract. 1st Nano Updates. *Arab. J. Chem.* **2012**, *5*, 431–437. [CrossRef]
35. Wilner, O.I.; Guidotti, C.; Wieckowska, A.; Gill, R.; Willner, I. Probing Kinase Activities by Electrochemistry, Contact-Angle Measurements, and Molecular-Force Interactions. *Chem. A Eur. J.* **2008**, *14*, 7774–7781. [CrossRef] [PubMed]
36. Radiom, M.; Yang, C.; Chan, W.K. Characterization of Surface Tension and Contact Angle of Nanofluids. In Proceedings of the Fourth International Conference on Experimental Mechanics, Singapore, 18–20 November 2009; SPIE: Bellingham, WA, USA, 2010; Volume 7522, pp. 395–403.
37. Abdelsalam, M.E.; Bartlett, P.N.; Kelf, T.; Baumberg, J. Wetting of Regularly Structured Gold Surfaces. *Langmuir* **2005**, *21*, 1753–1757. [CrossRef]
38. Noor, T.; Yaqoob, L.; Iqbal, N. Recent Advances in Electrocatalysis of Oxygen Evolution Reaction Using Noble-Metal, Transition-Metal, and Carbon-Based Materials. *ChemElectroChem* **2021**, *8*, 447–483. [CrossRef]
39. Raghav, J.; Deepak, D.; Sinha Roy, S.; Roy, S. Hybrid Nanostructure of Sputter Decorated Nanodots of Ag_2O/AgO over Flower-like Mn–Co–Cu Ternary Metal Oxide for Electrocatalytic Oxygen Evolution Reaction. *ACS Appl. Energy Mater.* **2023**, *6*, 2286–2295. [CrossRef]
40. Huang, X.; Li, H.; Li, J.; Huang, L.; Yao, K.; Yiu, C.K.; Liu, Y.; Wong, T.H.; Li, D.; Wu, M.; et al. Transient, Implantable, Ultrathin Biofuel Cells Enabled by Laser-Induced Graphene and Gold Nanoparticles Composite. *Nano Lett.* **2022**, *22*, 3447–3456. [CrossRef]
41. Rogers, C.; Perkins, W.S.; Veber, G.; Williams, T.E.; Cloke, R.R.; Fischer, F.R. Synergistic Enhancement of Electrocatalytic CO_2 Reduction with Gold Nanoparticles Embedded in Functional Graphene Nanoribbon Composite Electrodes. *J. Am. Chem. Soc.* **2017**, *139*, 4052–4061. [CrossRef]
42. Theerthagiri, J.; Lee, S.J.; Murthy, A.P.; Madhavan, J.; Choi, M.Y. Fundamental Aspects and Recent Advances in Transition Metal Nitrides as Electrocatalysts for Hydrogen Evolution Reaction: A Review. *Curr. Opin. Solid State Mater. Sci.* **2020**, *24*, 100805. [CrossRef]
43. Kibria, M.F.; Mridha, M.S.; Khan, A.H. Electrochemical Studies of a Nickel Electrode for the Hydrogen Evolution Reaction. *Int. J. Hydrogen Energy* **1995**, *20*, 435–440. [CrossRef]
44. Shin, S.; Jin, Z.; Kwon, D.H.; Bose, R.; Min, Y.-S. High Turnover Frequency of Hydrogen Evolution Reaction on Amorphous MoS_2 Thin Film Directly Grown by Atomic Layer Deposition. *Langmuir* **2015**, *31*, 1196–1202. [CrossRef]
45. Castro, E.B.; de Giz, M.J.; Gonzalez, E.R.; Vilche, J.R. An Electrochemical Impedance Study on the Kinetics and Mechanism of the Hydrogen Evolution Reaction on Nickel Molybdenite Electrodes. *Electrochim. Acta* **1997**, *42*, 951–959. [CrossRef]
46. Giesbrecht, P.K.; Freund, M.S. Investigation of Hydrogen Oxidation and Evolution Reactions at Porous Pt/C Electrodes in Nafion-Based Membrane Electrode Assemblies Using Impedance Spectroscopy and Distribution of Relaxation Times Analysis. *J. Phys. Chem. C* **2022**, *126*, 132–150. [CrossRef]
47. Xu, D.; Chan, K.C.; Guo, H.; Zhong, H.; Lu, L. One-Step Fabrication of a Laser-Induced Forward Transfer Graphene/Cu: XO Nanocomposite-Based Electrocatalyst to Promote Hydrogen Evolution Reaction. *J. Mater. Chem. A* **2021**, *9*, 16470–16478. [CrossRef]
48. Deng, H.; Zhang, C.; Xie, Y.; Tumlin, T.; Giri, L.; Karna, S.P.; Lin, J. Laser Induced MoS_2/Carbon Hybrids for Hydrogen Evolution Reaction Catalysts. *J. Mater. Chem. A* **2016**, *4*, 6824–6830. [CrossRef]

49. Khan, I.; Baig, N.; Bake, A.; Haroon, M.; Ashraf, M.; Al-Saadi, A.; Tahir, M.N.; Wooh, S. Robust Electrocatalysts Decorated Three-Dimensional Laser-Induced Graphene for Selective Alkaline OER and HER. *Carbon* **2023**, *213*, 118292. [CrossRef]
50. Lyu, L.; Kang, J.; Seong, K.; Kim, C.; Lim, J.; Piao, Y. ZnNiCo Hydroxide/Graphene-Carbon Nanotube Hydrogel on Surface-Modified Ni Foam as a Battery-Type Electrode for Hybrid Supercapacitors. *J. Alloys Compd.* **2021**, *872*, 159610. [CrossRef]
51. Kim, B.K.; Kim, M.J.; Kim, J.J. Impact of Surface Hydrophilicity on Electrochemical Water Splitting. *ACS Appl. Mater. Interfaces* **2021**, *13*, 11940–11947. [CrossRef]
52. Aguas, I.; Alarcón, E.; Villa, A.L. Turpentine Valorization by Its Oxyfunctionalization to Nopol through Heterogeneous Catalysis. *Heliyon* **2020**, *6*, e03887. [CrossRef] [PubMed]
53. Masoud, N.; Delannoy, L.; Calers, C.; Gallet, J.J.; Bournel, F.; de Jong, K.P.; Louis, C.; de Jongh, P.E. Silica-Supported Au–Ag Catalysts for the Selective Hydrogenation of Butadiene. *ChemCatChem* **2017**, *9*, 2418–2425. [CrossRef] [PubMed]